

Principles, Performance and Demonstration of an Up-conversion Time Microscope

C. V. Bennett

Dept. of Electrical Engineering, University of California, Los Angeles, and
Lawrence Livermore National Laboratory, P.O. Box 808, L-174, Livermore, California, 94551
cvbennett@llnl.gov

B. H. Kolner

Dept. of Applied Science, 228 Walker Hall, University of California, Davis,
Davis, California, 95616
kolner@leorg.ucdavis.edu

Abstract

The operational principles and performance limitations of up-conversion time microscopes are discussed and the results of a system demonstrating 103x magnification of femtosecond optical pulses are presented.

Principles, Performance and Demonstration of an Up-conversion Time Microscope

C. V. Bennett

Dept. of Electrical Engineering, University of California, Los Angeles, and
Lawrence Livermore National Laboratory, P.O. Box 808, L-174, Livermore, California, 94551
cvbennett@llnl.gov

B. H. Kolner

Dept. of Applied Science, 228 Walker Hall, University of California, Davis,
Davis, California, 95616
kolner@leorg.ucdavis.edu

Conventional technologies for recording single transient phenomena with ultrafast resolution have limitations on the total length of time and the complexity of the signals that can be recorded. Based on the theory of temporal imaging,¹ there exists a new approach for temporally expanding an unknown input waveform before it is recorded, thereby improving the resolution of the recording device. We have demonstrated a time microscope with 103x magnification which expanded an ultrafast input signal in time allowing it to be recorded with a photodiode and sampling oscilloscope with a total system resolution better than 300 fs.

Temporal imaging is based on an analogy that exists between paraxial diffraction and narrowband dispersion. Both are known to introduce a quadratic phase in their respective frequency domains, k_x, k_y or ω . In both cases this phase is acquired due to spatial propagation, scaling as d/k for diffraction and $\xi\beta''$ for dispersion, where d and ξ are propagation distances, k is the wavevector in the material, and β'' is the group velocity dispersion (GVD). A lens in space imparts a quadratic spatial phase, the strength of which is proportional to k/f , where the focal length f is a measure of the amount of diffraction required to remove the phase imparted by the lens. Likewise we may produce a time lens by imparting a quadratic temporal phase (or equivalently a linear frequency chirp $d\omega/d\tau$). A temporal focal distance ξ_f or focal group delay dispersion (GDD) $\phi_f'' = \xi_f\beta'' = -(d\omega/d\tau)^{-1}$ is defined as the amount of GDD required to remove the phase profile imparted by the lens. A temporal imaging system is produced by cascading an input GDD (ϕ_1''), a time lens, and an output GDD (ϕ_2''), in the proper balance to satisfy the temporal imaging condition $1/\phi_1'' + 1/\phi_2'' = 1/\phi_f''$. A temporally scaled replica of the input waveform is created at the output with magnification $M = -\phi_2''/\phi_1''$.

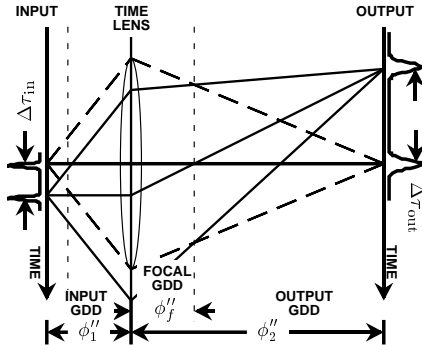


Fig. 1. Temporal ray diagram of a two-pulse sequence with $\phi_1'', \phi_2'', \phi_f'' > 0$ and $M = -3$.

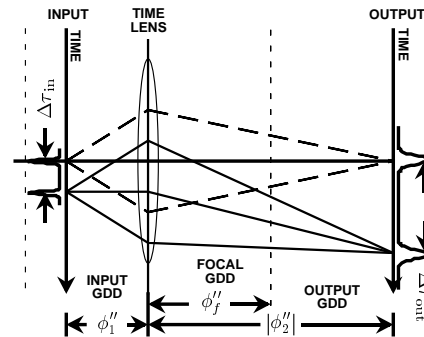


Fig. 2. Temporal ray diagram of a two-pulse sequence with $\phi_1'', \phi_f'' > 0, \phi_2'' < 0$ and $M = +3$.

[Note: Vertical axis in both figures is local time. Horizontal axis is propagation distance in units of GDD.]

Temporal “ray diagrams”² tracing the spectral components of input pulses suggest two possible imaging configurations. Since GDD (ϕ'') can be of either sign, a single lens temporal imaging systems can have either positive or negative magnification. For $M < 0$, all GDD must be of the same sign (Fig. 1). For $M > 0$, $\phi_1'', \phi_f'' > (<) 0$ and $\phi_2'' < (>) 0$ (Fig. 2). Both figures show two pulses at the same carrier frequency spreading as they propagate through the input GDD. The phase modulation process in the time lens frequency shifts each spectral component (ray) causing them to appear bent. The output GDD then focuses the rays creating a temporally scaled image.

The f -number of the time lens and thus the resolution of the temporal imaging system is inversely proportional to the bandwidth that is imparted by the modulation process; $f^\# = \omega_0/\Delta\omega$.¹ This provides

motivation for the up-conversion time lens³ which utilizes the broad bandwidth available from ultrashort light pulses to create a “fast” lens. A broad bandwidth linearly chirped pump pulse has the quadratic phase profile needed for a time lens and can be imparted to the input signal through mixing in a nonlinear crystal. The intensity profile of the pump acts like a temporal aperture through which an input signal must propagate and is a dominant determining factor for the temporal field of view.

One possible definition of the resolution of a temporal imaging system is that two pulses are “resolved” when they are separated at the output by the width of the system’s impulse response. For a Gaussian time lens pump pulse with perfectly linear frequency chirp and this definition of resolution it can be shown that the resolution referred to the input is $\delta\tau_{\text{in}} = .44 T f^{\#}$ or $\delta\tau_{\text{in}} \Delta f_{\text{pump}} = .44$ where T is an optical period and Δf_{pump} is the bandwidth of the pump. This definition of resolution may not be suitable for all applications but it shows that if our pump pulse is a dispersed pulse that was initially transform limited at around 100 fs it is reasonable to expect a temporal imaging system resolution near 100 fs.

There are a variety of potential aberration sources in temporal imaging systems. Higher order phase terms occur in the spectral phase of the dispersion networks as well as the temporal phase of the time lens. We have discovered that the dominant result of higher order spectral phase in the input of the system is to distort the shape of the system’s impulse response whereas when it is in the output it alters the arrival time of the impulse response. Time lens aberrations can produce a variety of effects including analogs to coma and spherical aberration in spatial systems. Phase matching in the nonlinear crystal is required for good conversion efficiency but group velocity mismatch between the fundamental and up-converted signal is often unavoidable. This leads to an increase in the width of the system’s impulse response and, more dramatically, an additional source of rolloff in the field of view. Our system was configured to minimize the effects of these aberrations and we are continuing to refine the aberration theory.

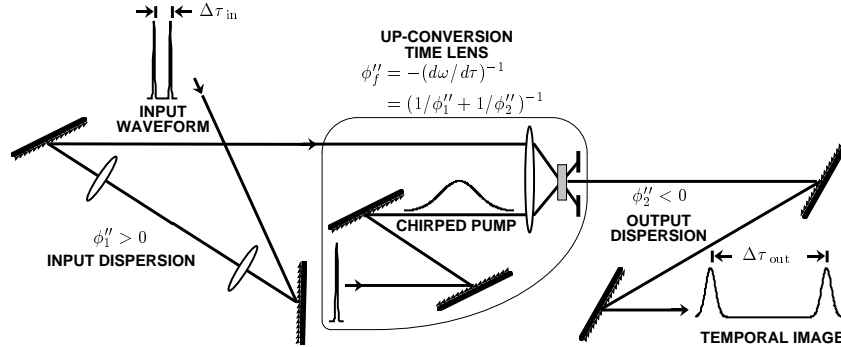


Fig. 3. Up-conversion time microscope with positive magnification. The input and output dispersions are constructed with grating pair dispersive delay lines. The time lens is produced by sum-frequency generation with a chirped optical pump pulse.

The system we have demonstrated is shown schematically in Fig. 3 and was designed for a magnification of $M = +100$, and field of view of ≈ 5 ps. A Ti:Sapphire laser producing 87 fs (5.0 THz) pulses at $\lambda = 830$ nm was used as the source for both the time lens pump and input test pattern. A two-pulse input test pattern with adjustable delay was created using a Michelson interferometer with minimum step size of 0.67 fs. The time lens was produced by dispersing a pulse in a folded multipass grating-pair dispersive delay line⁴ and mixing it with the dispersed input signal by noncollinear sum-frequency generation in a 500 μm thick BBO crystal. This pump pulse produced a time lens with an f -number of 82. The input and output GDD were also realized with folded multipass grating-pair dispersive delay lines, though lenses were used in the input to change the sign of the GDD.^{4,5} Both the input and pump dispersions used 600 g/mm gratings. The dispersions were characterized using “Spectrally Resolved Up-Conversion”⁶ and resulted in $\phi_1'' = +0.17606 \text{ ps}^2$, and a time lens with focal GDD $\phi_f'' = +0.17784 \text{ ps}^2$. The output GDD used a 3600 g/mm grating and was configured for $\phi_2'' = -17.606 \text{ ps}^2$.

Figure 4 shows a series of temporal images recorded with a 40 GHz photodiode and sampling oscilloscope. The output spectrum for each temporal image was also recorded and is shown in Fig. 5. Between each measurement the delay of pulse #2 was increased by $100.0 \pm 0.1 \mu\text{m}$ or 667 fs round trip. The right vertical axis in Figs. 4 and 5 is the input delay of the #2 pulse corresponding to each recorded output. The bottom axis in Fig. 4 is the actual photodiode signal time scale. A linear fit to the output vs. input time of pulse #2 gives a magnification of $M = +103$ with an error of 73 fs rms referred to the input. The top scale in Fig. 4 is an equivalent input timescale found by dividing the output time by the measured magnification. Temporal

images were also recorded in 100 fs delay steps near $\Delta\tau_{in} = 0$ fs. For delays as short as $\Delta\tau_{in} = 300$ fs two pulses are still clearly resolved in the temporal image. When the input delay is smaller the interference of the input pulses leave what is resolvable open to interpretation.

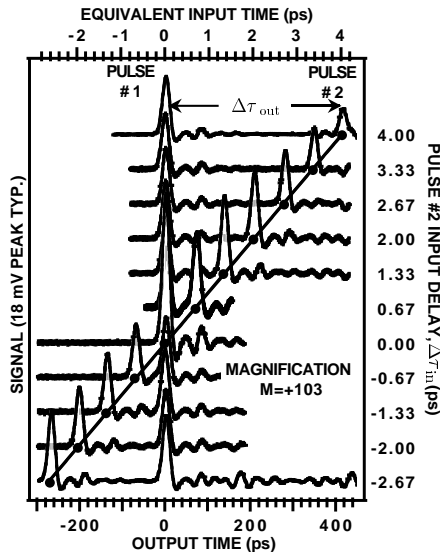


Fig. 4. Temporal images measured with 667 fs steps in the input delay of Pulse #2, $\Delta\tau_{in}$. Each output delay, $\Delta\tau_{out}$, changed by 68.7 ps, indicating a magnification of $M = +103$.

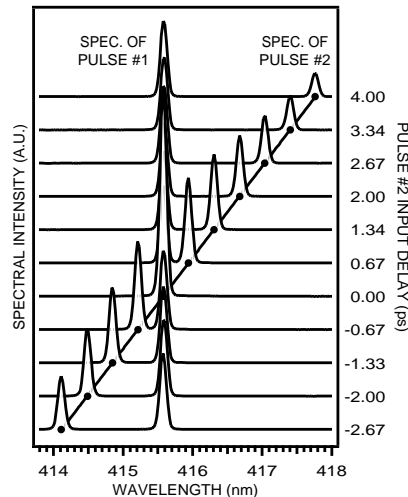


Fig. 5. Output spectra corresponding to the series of temporal images shown in Fig. 4. Linear frequency shift and symmetric spectral profile show no signs of significant input or lens aberrations.

The expected rolloff in the field of view is not readily apparent in Fig. 4. This could be masked by slight mechanical instabilities affecting the coupling into the photodiode. The spectral data of Fig. 5 clearly shows a Gaussian rolloff in the peak spectral intensity of pulse #2 as a function of input time, a fit to which gives an input temporal field of view of 5.65 ps FWHM, and is in good agreement with the width of the chirped time lens pump pulse.

The resolution and fidelity of the total system not only depends on the quality of the imaging system but also on the final recording device. Note that the impulse response of the photodiode (12.5 ps FWHM, with some ringing) is the dominant distortion in the total measurement system, **not** aberrations in the temporal imaging system itself. From a convolution of the ideal image, the ideal impulse response of the imaging system, and the measured impulse response of the photodiode, a 17.8 ps output pulse width was expected. The average measured width of pulse #2 in the images is 18.3 ps.

In conclusion, we have discussed many of the fundamental principles and performance issues for a temporal imaging system and demonstrated a system with +103x magnification and better than 300 fs resolution. In addition, since the principles of temporal imaging do not rely on sampling, it should be suitable for extending the range of single-shot waveform recording with optical streak cameras. It is expected that a scaling of this technology will lead to the realization of a new class of long record length, single transient recorders with ultrafast resolution.

This work was supported in part by the U.S. Department of Energy’s Lawrence Livermore National Laboratory under contract No. W-7405-Eng-48, the LLNL Photonics Group under LDRD grant No. 98-ERD-027, the National Science Foundation, the ATRI program of the US Air Force, and the David and Lucile Packard Foundation.

References

1. B. H. Kolner, *IEEE J. Quantum Electron.*, **30**, 1951 (1994).
2. S. P. Dijaili, A. Dienes, and J. S. Smith, *IEEE J. Quantum Electron.*, **26**, 1158 (1990).
3. C. V. Bennett, R. P. Scott, B. H. Kolner, *Appl. Phys. Lett.*, **65**, 2513 (1994).
4. E. B. Treacy, *IEEE J. Quantum Electron.*, **QE-5**, 454 (1969).
5. O. E. Martinez, J. P. Gordon, and R. L. Fork, *J. Opt. Soc. Am. A*, **1**, 1003 (1984).
6. J.-P. Foing, J.-P. Likforman, M. Joffre, and A. Migus, *IEEE J. Quantum Electron.*, **28**, 2285 (1992).